Korean J. Chem. Eng., **26**(4), 1144-1154 (2009)
DOI: 10.1007/s11814-009-0190-y

CFD simulation of coal-water slurry flowing in horizontal pipelines

Liangyong Chen, Yufeng Duan†, Wenhao Pu, and Changsui Zhao

School of Energy and Environment, Southeast University, Nanjing 210096, China
(*Received 29 July 2008 • accepted 5 January 2009*)

Abstract−An Eulerian multiphase approach based on kinetic theory of granular flow was used to simulate flow of coal-water slurries (CWS) in horizontal pipelines. The RNG k-ε turbulent model was incorporated in the governing equation to model turbulent two-phase flow with strong particle-particle interactions. In this model, the coal particles with bimodal distribution were considered as two solid-phase components, and the moment exchange between solid and liquid as well as that between solid and solid were accounted for. The model was firstly validated with pressure gradient and concentration profile data from the open literature, and then validated with pressure gradient data of the authors' experiments. The effects of influx velocity, total influx concentration and grain composition were numerically investigated, and the results have displayed some important slurry flow characteristics, such as constituent particle concentration distribution and velocity distribution as well as pressure gradients, which are very difficult to display in the experiments. The results suggest that both gravity difference between large and small particles and strong particle-particle interaction had significant effects on concentration distribution as well as velocity distribution.

Key words: Coal-water Slurry, High Concentration, Multi-fluid Model, Kinetic Theory of Granular Flow

INTRODUCTION

The transportation of highly concentrated coal-water slurries in pipelines is popular in numerous industrial applications ranging from coal combustion to gasification or liquefaction processes [1]. The most important technical parameters for designing a pipeline slurry transportation system are usually evaluated by empirical correlations or determined by experiments in a laboratory. However, flow behaviors of CWSs are very complex and the experimental investigations are difficult and expensive. The empirical correlations are usually developed based on limited data and their applicability is limited [2]. To develop a CFD model to predict those technical parameters such as pressure drop, velocity distribution, concentration distribution and others becomes the endeavor of the researchers.

With development of numerical technique and modeling of multiphase turbulent flow, numerical simulations of dense solid-liquid flow by Eulerian multiphase approach are becoming increasingly attractive [3]. The Eulerian model provides the most rational framework for describing such concentrated solid-liquid slurry flow. It accounts for liquid, particle and boundary interaction effects. In the Eulerian approach one is only required to give physical properties of liquid carrier and solids phase as well as operating conditions. The numerical investigations with this model have displayed some important slurry flow characteristics, such as concentration distributions, slurry density, slip velocity magnitude, velocity distributions, and slurry mean skin friction coefficient distributions, that is very difficult to display in the experiments. A CFD model within the framework of the Eulerian approach developed by Hsu [4] for flow of dense slurries through horizontal pipelines achieved great success. More recently, a numerical model based on space-time averaged multi-phase momentum conservation equations was developed by Assar [5], in which concentrations are obtained by solving governing equations derived from convective diffusion equation. Those approaches though successful, have a draw back that it needs many experimental coefficients or empirical equations to enclose the governing equation. Recently, many researchers used a mixture model, a simplified form of the Eulerian approach, to predict concentration and velocity distributions as well as pressure drop of slurry flow [6-8]. Its computation is relatively inexpensive and it is straightforward to introduce a turbulence model into the mixture model [8]. However, the mixture model does not account for effects of particle-particle interaction which extensively occur at high solid loading, so it is reasonably accurate for slurries with moderate volumetric concentrations.

In recent years, the Eulerian multiphase approach incorporated with kinetic theory of granular flow was applied to simulate super dense solid-liquid flow. In kinetic theory, solid phase behavior is analogous to the behavior of gas, and thus *a granular temperature* is defined to delineate solid phase fluctuations and transport properties. Because kinetic theory accounts for collisional and frictional characteristics of solid phase, it makes super dense solid-fluid flow tractable within the framework of Eulerian multiphase model. Many researchers use this framework to simulate solid-liquid flow behavior in a fluidized bed [9-13]. It is intended to predict accurate flow and other characteristics of liquid fluidized beds. A few studies [2, 14,15] use kinetic theory to predict flow behavior of dense slurry flow in pipelines. Although there have been enormous research efforts on two-phase slurry flow, there appear to be no numerical investigations on studies of super dense slurries such as CWSs. The total volume concentration of slurries investigated in the present work is much higher than those reported in the literature and the average volume concentration is up to more than 50%. Thus, it is necessary to consider both large-scale fluctuations due to mixture

†To whom correspondence should be addressed.
E-mail: yfduan@seu.edu.cn
‡This work was presented at the 7th Korea-China Workshop on Clean Energy Technology held at Taiyuan, China, July 25-28, 2008.

turbulence and small-scale fluctuations due to particle-particle collision. In addition, the solid phase of CWSs usually exhibits bimodal distribution. It is more rational to consider the solid phase as two components according to two peaks of particle size distribution and the moment exchange between different solid phases needs to be included. At present, only few studies [16,17] have reported experimental results on double-solid-phases slurry flow. Our numerical results show more important flow characteristics than these reported.

We extended the limited earlier work on application of Eulerian multiphase approach with kinetic theory of granular flow to predict flow behaviors of CWSs in horizontal pipelines. The RNG k-ε turbulent model was incorporated in the governing equation to model solid-liquid two phase turbulent flow with strong particle-particle interaction in a wide range of Reynolds number. In simulations, the coal particles with bimodal distribution were subdivided into two particle components and drag forces between solid and liquid, solid and solid were taken into account. The model was validated with pressure drop data from our experiments as well as pressure gradient and concentration profile data from the open literature. The effects of influx velocity, total influx concentration and grain composition on constituent particles concentration and velocity distribution were investigated.

MATHEMATICAL MODELS

1. Governing Equations

In Eulerian multiphase approaches, the macroscopic balance equations of mass, momentum conservation are solved for each phase. The continuity and momentum equations for liquid and solid phase can be written as:

$$\frac{\partial}{\partial t}(\alpha_f\rho_f)+\nabla\cdot(\alpha_f\rho_f\mathbf{u}_f)=0 \tag{1a}$$

$$\frac{\partial}{\partial t}(\alpha_{si}\rho_{si})+\nabla\cdot(\alpha_{si}\rho_{si}\mathbf{u}_{si})=0 \tag{1b}$$

$$\frac{\partial}{\partial t}(\alpha_f\rho_f\mathbf{u}_f)+\nabla\cdot(\alpha_f\rho_f\mathbf{u}_f\mathbf{u}_f)=-\alpha_f\nabla P+\nabla\cdot\tau_f+\sum_{i=1}^{2}\beta_{fi}(\mathbf{u}_{si}-\mathbf{u}_f)+\alpha_f\rho_f\mathbf{g} \tag{2a}$$

$$\frac{\partial}{\partial t}(\alpha_{si}\rho_{si}\mathbf{u}_{si})+\nabla\cdot(\alpha_{si}\rho_{si}\mathbf{u}_{si}\mathbf{u}_{si})=-\alpha_{si}\nabla P-\nabla P_{si}+\nabla\cdot\tau_{si}+\beta_{fi}(\mathbf{u}_f-\mathbf{u}_{si})+\beta_{ji}(\mathbf{u}_{sj}-\mathbf{u}_{si})+\alpha_{si}\rho_{si}\mathbf{g} \tag{2b}$$

$$\sum_{i=1}^{2}\alpha_{si}+\alpha_f=1 \tag{3}$$

where α_f, ρ_f and $\mathbf{u}_f$ are volume fraction, density and velocity of liquid phase, respectively; α_{si}, ρ_{si} and $\mathbf{u}_{si}$ are volume fraction, density and velocity of ith component of solid phase, respectively; ∇P and ∇P_{si} are pressure shared by all phase and collisional solid stress that represent additional stress in solid phase due to particle collisions. β_{fi} and β_{ji} are moment exchange coefficients of liquid-solid and solid-solid flow; $\nabla\cdot\tau_f$ and $\nabla\cdot\tau_{si}$ are viscous stress tensors of liquid and solid phase. For liquid phase:

$$\tau_f=\alpha_f\mu_{f,eff}[\nabla\mathbf{u}_f+(\nabla\mathbf{u}_f)^T]-\frac{2}{3}\alpha_f\mu_{f,eff}(\nabla\cdot\mathbf{u}_f)\mathbf{I} \tag{4}$$

where $\mu_{f,eff}=\mu_f+\mu_{t,f}$; μ_f and $\mu_{t,f}$ are liquid molecular viscosity and turbulence viscosity.

2. Interphase Momentum Exchange

The model for exchange coefficient β_{fi} is formulated as Eq. (5) [18]:

$$\beta_{fi}=\begin{cases}\dfrac{150\alpha_{si}\alpha_f\mu_f}{\alpha_f d_{si}^2}+1.75\dfrac{\rho_f\alpha_{si}}{d_{si}}|\mathbf{u}_{si}-\mathbf{u}_f| & \text{if } \alpha_f\le 0.8\\ \dfrac{3}{4}C_D\dfrac{\alpha_{si}\rho_f|\mathbf{u}_{si}-\mathbf{u}_f|}{d_{si}}\alpha_f^{-2.65} & \text{if } \alpha_f>0.8\end{cases} \tag{5}$$

According to Syamlal [19], drag fore between two different solid phases is given by:

$$\beta_{ij}=\frac{3(1+e_{ij})\left(\frac{\pi}{2}+C_{fr,ij}\frac{\pi^2}{8}\right)\alpha_{si}\rho_{si}\alpha_{si}\rho_{si}(d_{si}+d_{sj})^2 g_{0,ij}}{2\pi(\rho_{si}d_{si}^3+\rho_{sj}d_{sj}^3)}|\mathbf{u}_{si}-\mathbf{u}_{sj}| \tag{6}$$

Where e_{ij} is restitution coefficient between ith and jth solid phase. d_{si} and d_{sj} are the diameter of particles of ith and jth solid phase, respectively. $C_{fr,ij}$ is the friction coefficient taken as 0.15 in the present work.

3. Constitutive Equation of Solid Phase

The constitutive equations of solid phases are based on kinetic theory for granular flow. Analogous to thermodynamic temperature in a gas, granular temperature for solid phase can be defined as [20]:

$$\Theta_s=\frac{1}{3}\langle\mathbf{c}^2\rangle \tag{7}$$

hereis $\langle\mathbf{c}^2\rangle$ the mean square of fluctuation velocity of particles, $\mathbf{c}=\mathbf{u}_s-\langle\mathbf{u}_s\rangle$.

The transport equation for granular temperature based on conservation of particles fluctuating energy is given by [21]:

$$\frac{3}{2}\left[\frac{\partial}{\partial t}(\rho_{si}\alpha_{si}\Theta_{si})+\nabla\cdot(\rho_{si}\alpha_{si}\mathbf{u}_{si}\Theta_{si})\right]=(-P_{si}\mathbf{I}+\tau_{si}):\nabla\mathbf{u}_{si}+\nabla\cdot(K_{\Theta si}\nabla\Theta_{si})-\gamma_{\Theta si}+\phi_{fsi}+D_{fsi} \tag{8}$$

The first term on the right-hand side of this equation represents rates of production of pseudo-thermal energy by shear; the second represents diffusive transport of pseudo-thermal energy. $\gamma_{\Theta si}$ represents dissipation of pseudo-thermal energy through inelastic collisions, ϕ_{fsi} denotes exchange of fluctuating energy between fluid and ith component of solid phase, D_{fsi} is granular energy dissipation rate, $K_{\Theta si}$ is granular conductivity. They are defined as [18]:

$$K_{\Theta si}=\frac{150\rho_{si}d_{si}\sqrt{\Theta_{si}\pi}}{384(1+e_{ii})g_{0,ii}}\left[1+\frac{6}{5}\alpha_{si}g_{0,ii}(1+e_{ii})\right]^2+2\alpha_{si}^2\rho_{si}d_{si}g_{0,ii}(1+e_{ii})\sqrt{\frac{\Theta_{si}}{\pi}} \tag{9}$$

$$\gamma_{\Theta si}=3(1-e_{ii}^2)g_{0,ii}\rho_{si}\alpha_{si}^2\Theta_{si}\left(\frac{4}{d_{si}}\sqrt{\Theta_{si}/\pi}-\nabla\mathbf{u}_{si}\right) \tag{10}$$

$$\phi_{fsi}=-3\beta_{fi}\Theta_{si} \tag{11}$$

$$D_{si}=\frac{d_{si}\rho_{si}}{4\sqrt{\pi\Theta_{si}}}\left(\frac{18\mu_f}{d_{si}^2\rho_{si}}\right)^2|\mathbf{u}_f-\mathbf{u}_{si}|^2 \tag{12}$$

P_{si} is given by [22]:

$$P_{si}=\rho_{si}\alpha_{si}\Theta_{si}+\sum_{j=1}^{2}2\frac{d_{ij}^3}{d_{si}^3}(1+e_{ij})\rho_{si}\Theta_{si}g_{0,ij}\alpha_{si}\alpha_{sj} \quad (13)$$

where $g_{0,ii}$ and $g_{0,ij}$ are radial distribution functions and the following expressions are adopted [23]:

$$g_{0,ii}=\left[1-\left(\sum_{i=1}^{2}\alpha_{si}/\alpha_{s,max}\right)^{1/3}\right]^{-1}+0.5d_{si}\sum_{k=1}^{2}\frac{\alpha_{sk}}{d_{sk}} \quad (14)$$

$$g_{0,ij}=\frac{d_{si}g_{0,ii}+d_{sj}g_{0,jj}}{d_{si}+d_{sj}} \quad (15)$$

where $\alpha_{s,max}$ is the maximum packing fraction of the mixture.

The solid phase is dealt with a Newtonian fluid behavior and τ_{si} is given by:

$$\tau_{si}=\alpha_{si}\mu_{si}[\nabla\mathbf{u}_{si}+(\nabla\mathbf{u}_{si})^T]+\alpha_{si}\left(\lambda_{si}-\frac{2}{3}\mu_{si}\right)(\nabla\cdot\mathbf{u}_{si})\mathbf{I} \quad (16)$$

where μ_{si} and λ_{si} are shear and bulk solid viscosity. They are defined as [18,22]:

$$\mu_{si}=\frac{4}{5}\alpha_{si}\rho_{si}d_{si}g_{0,ii}(1+e_{ii})\left(\frac{\Theta_{si}}{\pi}\right)^{1/2}+\frac{10\rho_{si}d_{si}\sqrt{\Theta_{si}\pi}}{96\alpha_{si}(1+e_{ii})g_{0,ii}}\left[1+\frac{4}{5}\alpha_{si}g_{0,ii}(1+e_{ii})\right]^2 \quad (17)$$

$$\lambda_{si}=\frac{4}{3}\alpha_{si}\rho_{si}d_{si}g_{0,ii}(1+e_{ii})\left(\frac{\Theta_{si}}{\pi}\right)^{1/2} \quad (18)$$

4. Turbulence Model

The homogeneous approach was employed where both phases are assumed to share the same values for k and ε. The RNG k-ε turbulent mixture model is used in this study, which allows the model to better handle low Reynolds number and near wall flows than the standard k-ε turbulent model.

$$\frac{\partial}{\partial t}(\rho_m k)+\nabla\cdot(\rho_m\mathbf{u}_m k)=\nabla\cdot(a_k\mu_{m,eff}\nabla k)+\mu_{m,t}S^2-\rho_m\varepsilon \quad (19a)$$

$$\frac{\partial}{\partial t}(\rho_m\varepsilon)+\nabla\cdot(\rho_m\mathbf{u}_m\varepsilon)=\nabla\cdot(a_\varepsilon\mu_{m,eff}\nabla\varepsilon)+C_{1\varepsilon}\frac{\varepsilon}{k}\mu_{m,t}S^2-C_{2\varepsilon}\rho_m\frac{\varepsilon^2}{k}-E_\varepsilon \quad (19b)$$

where a_k and a_ε are the inverse effective Prandtl number for k and ε, respectively. In high Reynolds number limit, $a_k=a_\varepsilon\approx1.393$. $C_{1\varepsilon}$ and $C_{2\varepsilon}$ are equal to 1.42 and 1.68. S is modulus of the mean rate-of-strain tensor. E_ε is given by $E_\varepsilon=(C_\mu\rho\eta^3(1-\eta/\eta_0))/(1+\zeta\eta^3)\ \varepsilon^2/k$, $\eta=S\cdot k/\varepsilon$, $\eta_0\approx4.38$, $\zeta=0.012$, $C_\mu=0.085$. ρ_m and $\mathbf{u}_m$ are mean density and mean velocity of the mixture.

5. Boundary Conditions

The fluid and solid particles' velocity distribution at the inlet was treated as uniform and the solid particles evenly distributed. The continuous phase was assumed to obey a no slip boundary condition at the wall and the standard wall functions were specified. Partial slip boundary conditions for particle-wall interaction proposed by Johnson and Jackson were applied [24].

$$\tau_{sw}=\frac{\sqrt{3}}{6}\pi\rho_{si}g_{0,ii}\varphi\frac{\alpha_s}{\alpha_{s,max}}\sqrt{\Theta_{si}}\mathbf{u}_{siw} \quad (20)$$

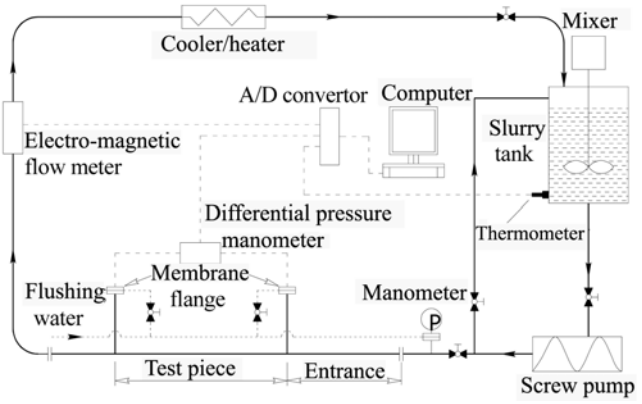

Fig. 1. Schematic diagram of experimental setup.

$$q_{wi}=\frac{\sqrt{3}}{6}\pi\rho_{si}g_{0,ii}\varphi\frac{\alpha_s}{\alpha_{s,max}}\sqrt{\Theta_{si}}\mathbf{u}_{siw}\cdot\mathbf{u}_{siw}-\frac{\sqrt{3}}{4}\pi\rho_{si}g_{0,ii}(1-e_{siw}^2)\frac{\alpha_s}{\alpha_{s,max}}\Theta_{si}^{3/2} \quad (21)$$

Where $\mathbf{u}_{siw}$ is particle slip velocity parallel to the wall, φ is the specularity coefficient representing the fraction of total momentum transferred to the wall when particle collides with it, q_{wi} is flux of granular temperature toward the wall, and e_{siw} is restitution coefficient of particle-wall collision.

EXPERIMENTS AND NUMERICAL COMPUTATION

1. Experiments

The numerical simulations were mainly based on our experimental investigations on resistance properties of CWSs flowing in a set of horizontal pipes. Experiments were performed on a pilot scale slurry transport apparatus (at the School of Energy and Environment, Southeast University of China). A schematic diagram of experimental set-up is shown in Fig. 1. It consists of a storage/preparation part, a test loop, measuring devices and a data acquisition system. The tested coal-water slurries were prepared and stored in the slurry tank. A stirring device was mounted on the top of the slurry tank. During testing, the slurries were under stirring to prevent settling of solid particles and the slurry tank was well covered to prevent water loss. The driving force for pumping test slurries was provided by a screw pump with a rated flow rate of 16 m^3/h, driven by a YCT motor. The flow properties of test slurries were characterized by steel pipes with various inner diameters (25 mm, 32 mm, 40 mm and 50 mm). For each diameter, the test section was 2.2 m long and a sufficient entrance before the test section was used to eliminate entrance effects. The flow rate Q and the pressure drop ΔP were measured by an electro-magnetic flow meter and electric differential-pressure manometer, respectively. Both signals were converted from analog to digital by an A/D converter and then recorded in a computer database for later retrieval and analysis. The slurry temperature was controlled by a heat exchanger incorporated in the end of the test loop. At each test, the slurry temperature was maintained at the required level with deviation less than 1, and the signals of the slurry temperature were recorded on-line during testing.

The effects of influx velocity, slurry temperature, pipe diameter

Table 1. Parameters of test slurries and operating conditions

Solid density /(g/cm^3)	Mean particle size/μm	Total influx concentration/%	Test pipe diameter /mm	Slurry temperature
1.465	134.5	30	32	20
		41.7	25, 32, 40, 50	20
		49.5	25, 32, 40, 50	20, 52
		53.8	32	20, 52

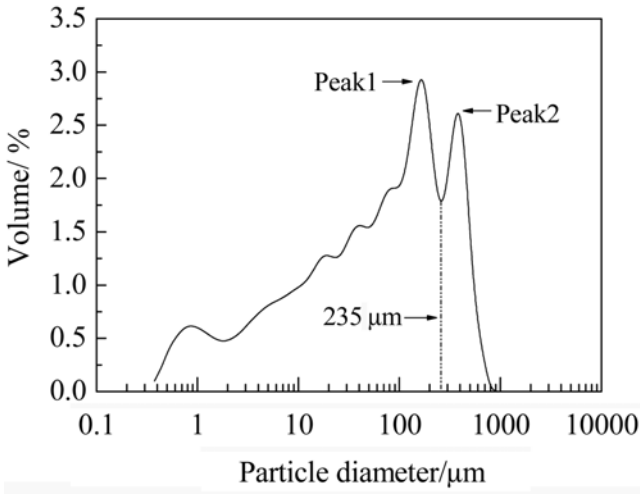

Fig. 2. Particle size distribution of coal particles.

and total influx concentration on pressure drop were investigated. The operating conditions and the parameters of the test slurries are listed in Table 1. Effects of influx volume fraction were investigated at four different level ranged from 30% to 53.8%. Effects of temperature were investigated at 20 °C and 52 °C for 49.5% and 53.8% CWSs. The test slurries were self prepared by mixing coal powder with tap water in slurry tank. During testing, slurries were under stirring to keep homogeneous at the entrance of test pipe. For each test, new prepared slurries were used. Measurement was repeated two or three times for more accuracy. Coal particles contained in slurries have an average diameter 134.5 μm and the particle size distributions are shown in Fig. 2. In numerical simulation, the solid phase was regard as a binary mixture of 65 μm and 345 μm pulverized coal according to two peaks as shown in Fig. 2, and the volume ratio of the small to the large particles was taken as 3 : 1.

2. Numerical Methods

In numerical investigations, the flows were considered as steady three-dimensional flow and the effects of viscous heating were negligible. The second-order upwind scheme was selected as the discretization scheme in all governing equations and the phase-coupled SIMPLE iterative algorithm was used to resolve the coupling between velocity and pressure. To avoid divergence, under-relaxation technique was applied. The under-relaxation factor for pressure was 0.2-0.3, for momentum was 0.5-0.7, for granular temperature was 0.1-0.2, and these for turbulence kinetic energy and its dispassion rate were 0.7-0.8. The convergence criteria were set at 10^{-4} for all equations except for the granular temperature equation which residual was set at 10^{-3}. A computational domain L≥200D was used to ensure fully developed flow results could be obtained for all pipes. Owing to symmetry, it would be possible to model only a half of the pipe. Tests were done to study the effects of mesh size on simulation results, and the investigations revealed that 8×16×800 cells showed mesh-independent results. The values of restitution coefficient and packing limit of solid particles have significant effects on simulation results and must be selected with great care. In our investigations, all coefficients of restitution among particles and between particle and solid boundary were set at 0.7-0.95. The packing limits for coarse and fine particles were all estimated as 0.65.

RESULTS AND DISCUSSIONS

1. Comparison of Numerical and Experimental Results

The present CFD model was firstly validated with experimental data from reference [15]. Kaushal's experiments were conducted in 54.9 mm diameter horizontal pipe, and the pressure drop and concentration profiles were measured. The slurries had been prepared by mixing 125 μm and 440 μm spherical glass beads with water. The spherical glass beads have a mean density of 2,470 kg/m^3 and the volume ratio of the fine to coarse particles was 50 : 50 in the prepared slurries. Fig. 3 depicts the comparison of pressure gradients along the axis obtained from our CFD model with those of Kaushal's experiments. The numerical pressure gradients basically agree well with the experimental results at all velocities. Only at velocity (V= 1 m/s) lower than the corresponding critical deposition velocity of slurry flow do the data points appear to have an error of more than 20%. Fig. 4(a)-(d) show the comparisons between the model predicted and measured total volume concentration profiles along the vertical diameter at various influx velocities. Both the numerical and experimental data show that the total volume concentrations increase from top to bottom of the pipe when influx velocity is lower than 5 m/s. At an influx velocity of 5 m/s, the values of total volume concentration are almost the same at all heights. It is obvious that the experimental data lie around the lines of the numerical results

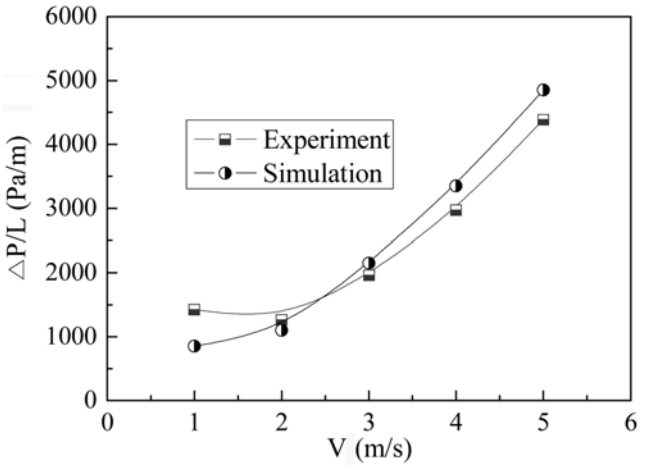

Fig. 3. Comparisons of numerical pressure gradients with those of Kaushal's experiments for slurries of the mixture of 125 μm and 440 μm particle sizes at 40% total influx concentration.

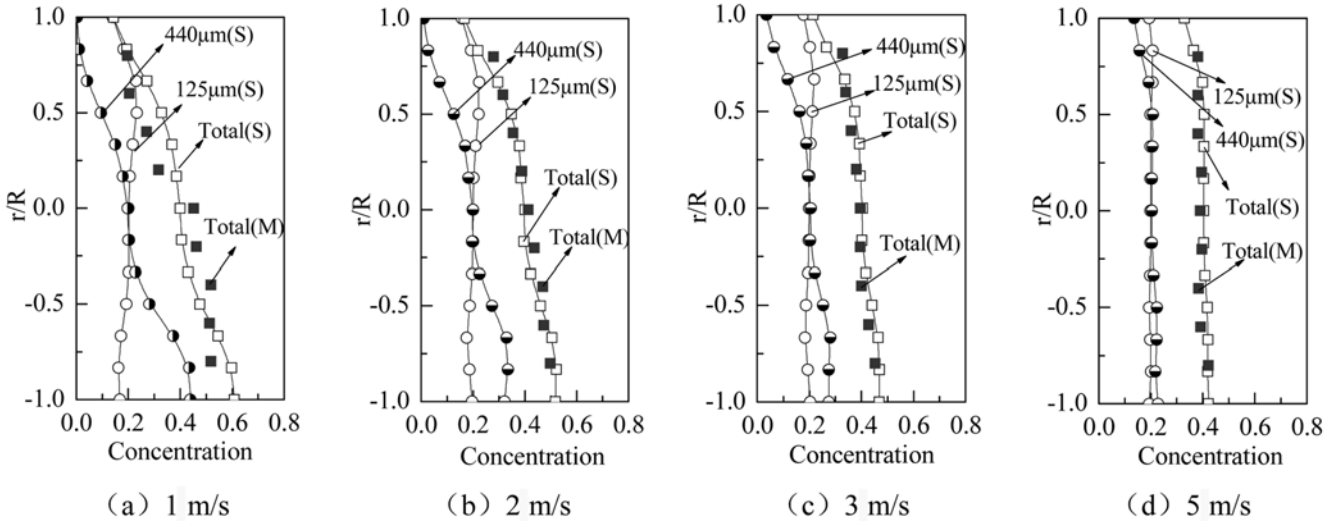

Fig. 4. Comparisons of numerical concentration profiles along vertical diameter with those of Kaushal's experiments for slurries of the mixture of 125 μm and 440 μm particle sizes at 40% total influx concentration (S-Simulation; M-Measurement).

with perfect agreement, and the accuracy of the predictions is slightly dependent on the influx velocities. Fig. 4(a)-(d) also give the calculated constituent particles concentrations along the vertical diameters. The concentrations of larger particles along the vertical diameters vary considerably at low influx velocities, and the fine particles are distributed more uniformly at all height for various influx velocities. Those numerical data reasonably agree with Kaushal's results, although he did not give the detailed constituent particle concentration distributions for all influx velocities investigated. It can be concluded from the above discussion that the present CFD model can be used with confidence in predicting flow properties of slurries with solid particle having a bimodal distribution.

The numerical results from the CFD model were also checked and validated with the mean pressure gradient of our experiments over a wide range of operating conditions. Comparisons of experimental pressure drops with numerical data for 49.5% CWSs in different pipes and those for 49.5% and 53.8% CWSs at temperature of 20 °C and 50 °C are shown by Fig. 5(a) and (b) respectively. The discrete points and the corresponding solid curves represent experimental data and numerical results, respectively. Clearly, all numerical results are in good agreement with experimental data. The mean fraction deviations between the numerical and experiment results are less than 20%, which is much lower than the predictive error of 25-50% with empirical correlations for pressure drops.

In Fig. 5(b) the experimental data shows that the fluidity of 53.8% CWSs at temperature of 20 °C and 50 °C greatly decreases when compared with that of lower concentrations. The biggest discrepancies between the numerical results and experiment data take place in the low range of influx velocities. When volume concentration of solid particles approximates to its maximum packing fraction, the flow regime of slurries becomes under control of solid motion and these effects of properties of solid particles such as solid shape come into play. However, non-spherical effects of coal particles are not under consideration in the CFD model in which the solid particles are considered as spherical ones with the same diameters. Thus, numerical results from the CFD model result in under-prediction

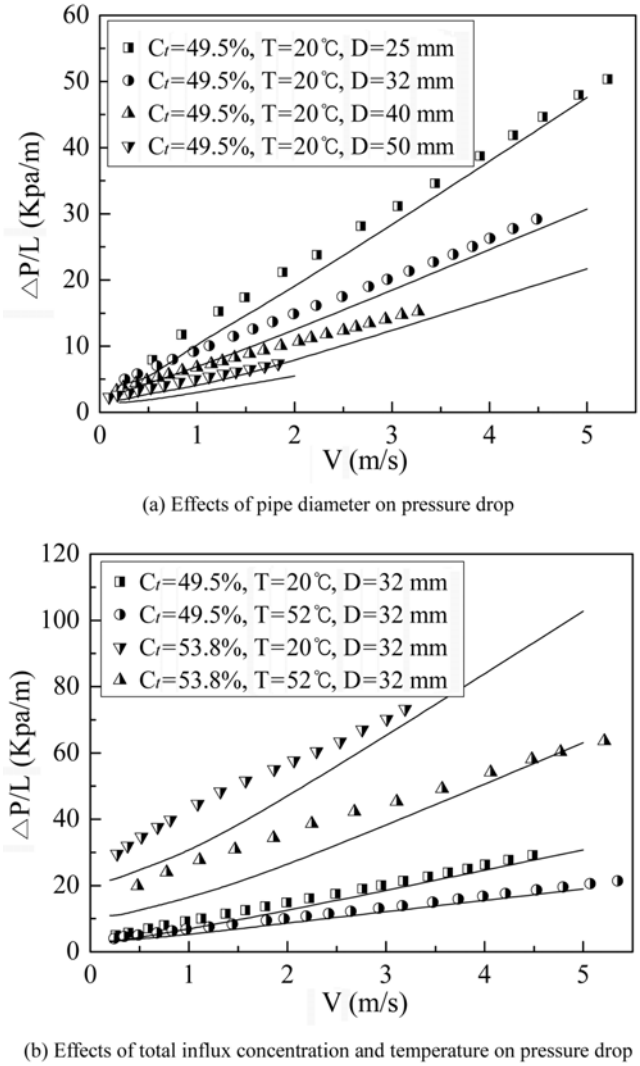

Fig. 5. Comparisons of numerical and experimental pressure gradients for CWSs.

compared with the experimental data. It should be pointed out that the discrepancies between the two would be greatly decreased at high influx velocities. For slurries with concentrations lower than 50%, the numerical results also lead to a little underestimation of pressure gradients in the low range of influx velocities. At low flow velocities, the amount of solid particles at the low part of the pipe increases due to gravitational effects. Similar to super dense slurries, the effects of shape of solid particles cause more energy losses in suspensions than the predictive results. However, the relative deviation between the simulation and experimental results did not exceed 10% because additional pressure losses are only confined to the area of bottom of the pipe.

2. Concentration and Velocity Distributions in Vertical Plane

The volume concentration distribution of components and velocity distribution are mainly affected by influx velocity and total influx concentration of solid phases. Fig. 6 and Fig. 7 show volume concentration distribution of components and velocity distribution in vertical plane at influx velocity of 0.2 m/s and 0.5 m/s for 49.5% CWSs, respectively. Here, the mean velocity of the mixture is selected to present slurry velocity because the slip velocity between solid and liquid phase is so small to be negligible. It is observed that coarse particle concentration varies considerably along the vertical height due to gravitational force, while 65 μm particles are slightly more uniformly distributed. The slurry velocities near the wall drop down sharply due to strong viscous shear stress. The velocity profiles become distorted from a circular shape due to the nonuniform distribution of solid phases in the cross-sectional area of the pipe. It also shows that increasing influx velocity leads to increase of uniformity of solid phase distribution, and the shape of constant velocity contour curve becomes less distorted from a circular shape.

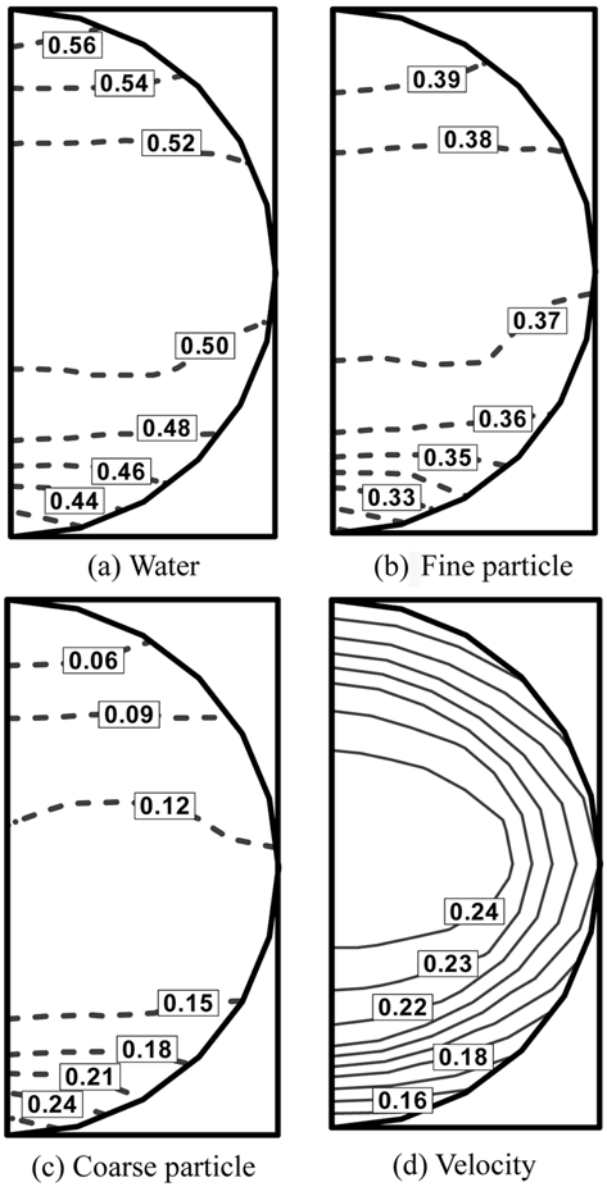

Fig. 6. Volume concentration distributions of components and velocity distribution in vertical plane at influx velocity of 0.2 m/s for 49.5% CWSs.

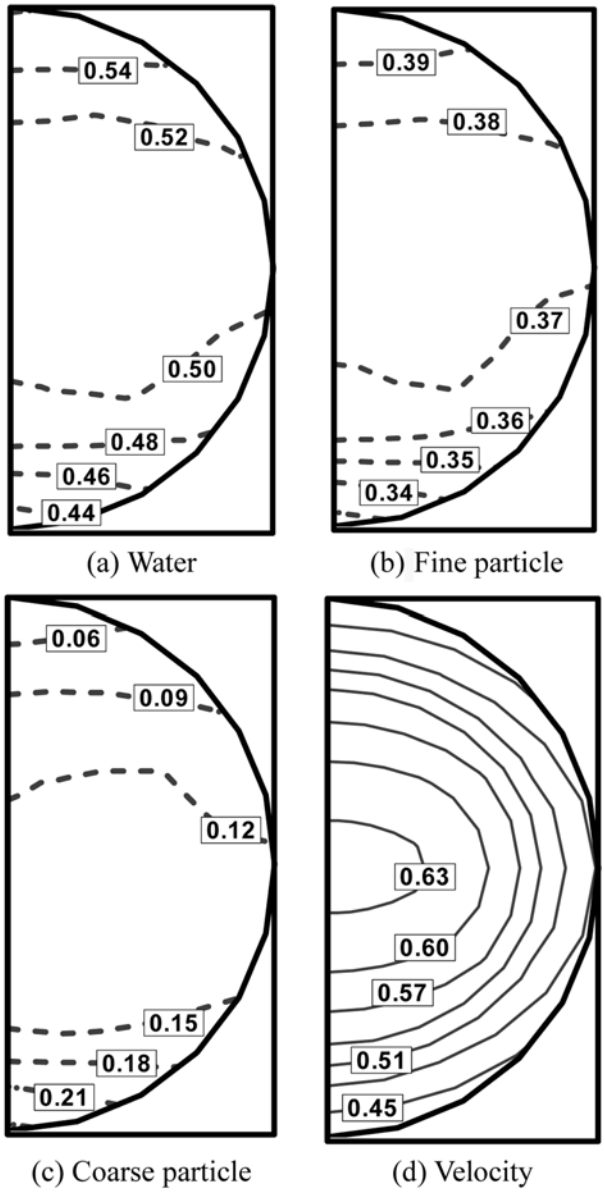

Fig. 7. Volume concentration distributions of components and velocity distribution in vertical plane at influx velocity of 0.5 m/s for 49.5% CWSs.

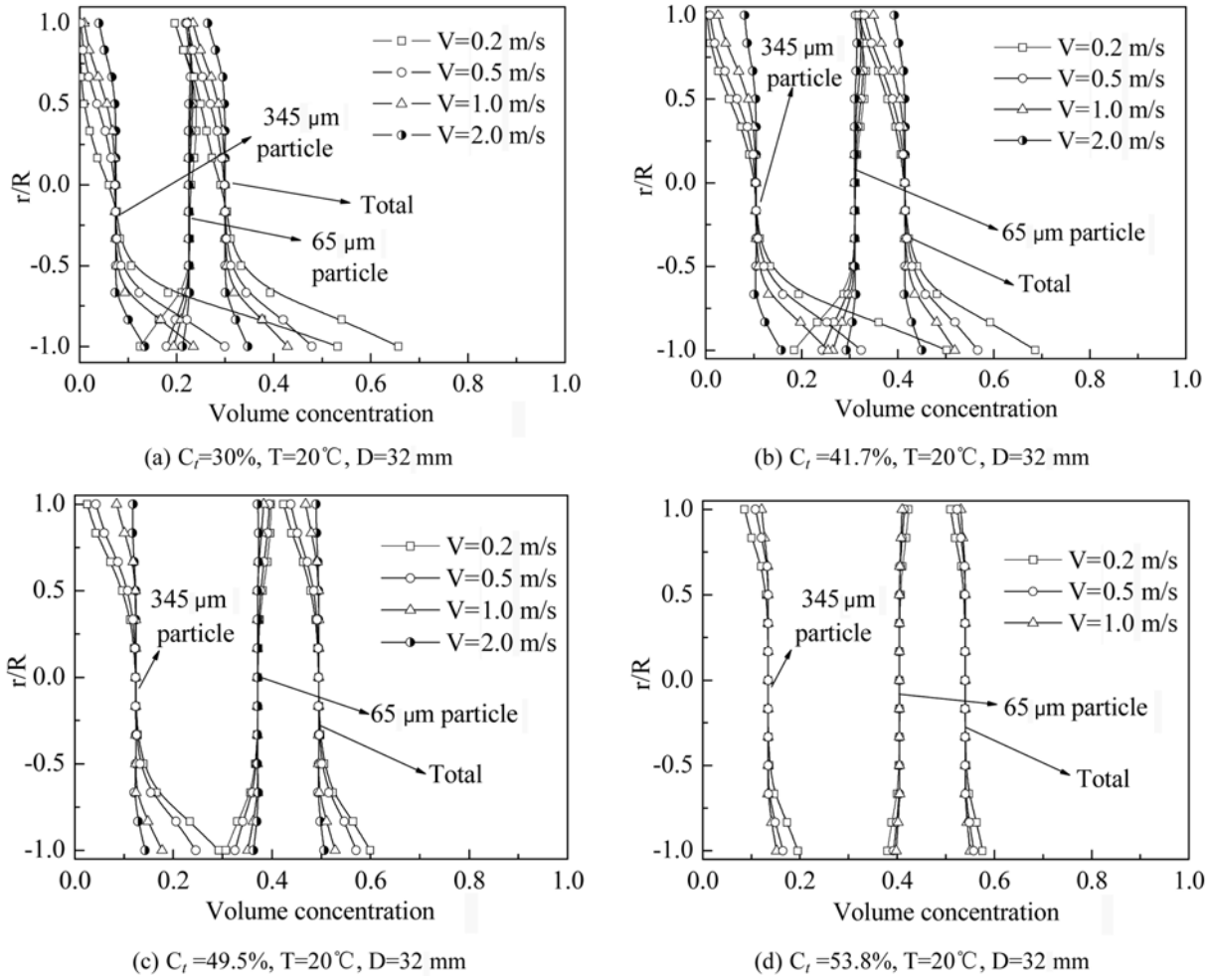

Fig. 8. Volume concentration distribution along the vertical diameter.

3. Concentration Profile

Fig. 8(a)-(d) depicts the calculated constituent particle concentrations and total volume concentrations along the vertical diameters in the fully developed region for slurries at various influx velocities and total influx concentrations, by volume concentration vs. r/R, with r being the distance from the pipe center and R being the pipe radius. From Fig. 8(a)-(c), it is observed that the total volume concentration distribution of solid phases shows large gradient along the vertical diameter because of gravitational effects in the low range of influx velocities, which indicates that the flow of slurries belongs to heterogeneous regime. It is also observed that the distributions of total volume concentration at various influx velocities are similar to each other for the same slurries. In the central part of the pipeline, the total volume concentration is slightly higher than the total influx concentrations and is almost kept constant when influx velocity is increased. On the top of the pipeline, the total volume concentration is lower than its total influx concentration and decreases gradually with increasing r/R. However, in the low part of the pipeline, the same tendency has been observed but the gradient of total volume concentration is higher than that on the top of the pipeline. This suggested that for our slurries with solid phase having bimodal distribution, the total volume concentration profile along the vertical diameter is similar to that of slurries with single solid phase [3].

Fig. 8(a) shows that there are large gradients of total volume concentration on the top and bottom of pipelines for 30% slurries with V=0.2 m/s, and the degree of uniformity of solid distribution along the vertical diameter increases with increase in influx velocity. This is expected because with increase in influx velocity there will be an increase in turbulent energy, which is a main responsibility for keeping solid suspended. For a given influx velocity, increasing concentration enhances uniformity of solid distribution due to enhanced interference effects between solid particles. Fig. 8(d) shows that 53.8% slurries keeps almost homogeneous flow even at very low influx velocity, which suggests that the interaction and interference effects between solid particles become the controlling factor of slurry flow. From Fig. 8(a)-(d), it is observed that for a given influx velocity, the central region with zero total volume concentration gradient expands with increasing total influx concentration. Simultaneously, the region with lower concentration on the top of the pipeline is contracted, while the region with higher concentration in the low part of pipeline remains almost unchanged, which occupies 1/4 height in the vertical diameter. Another surprising finding is that increasing influx velocity enhances the uniformity of solid distribution, while the sizes of three regions keep almost invariant.

It is clear in Fig. 8(a)-(c) that the concentrations of 345 μm par-

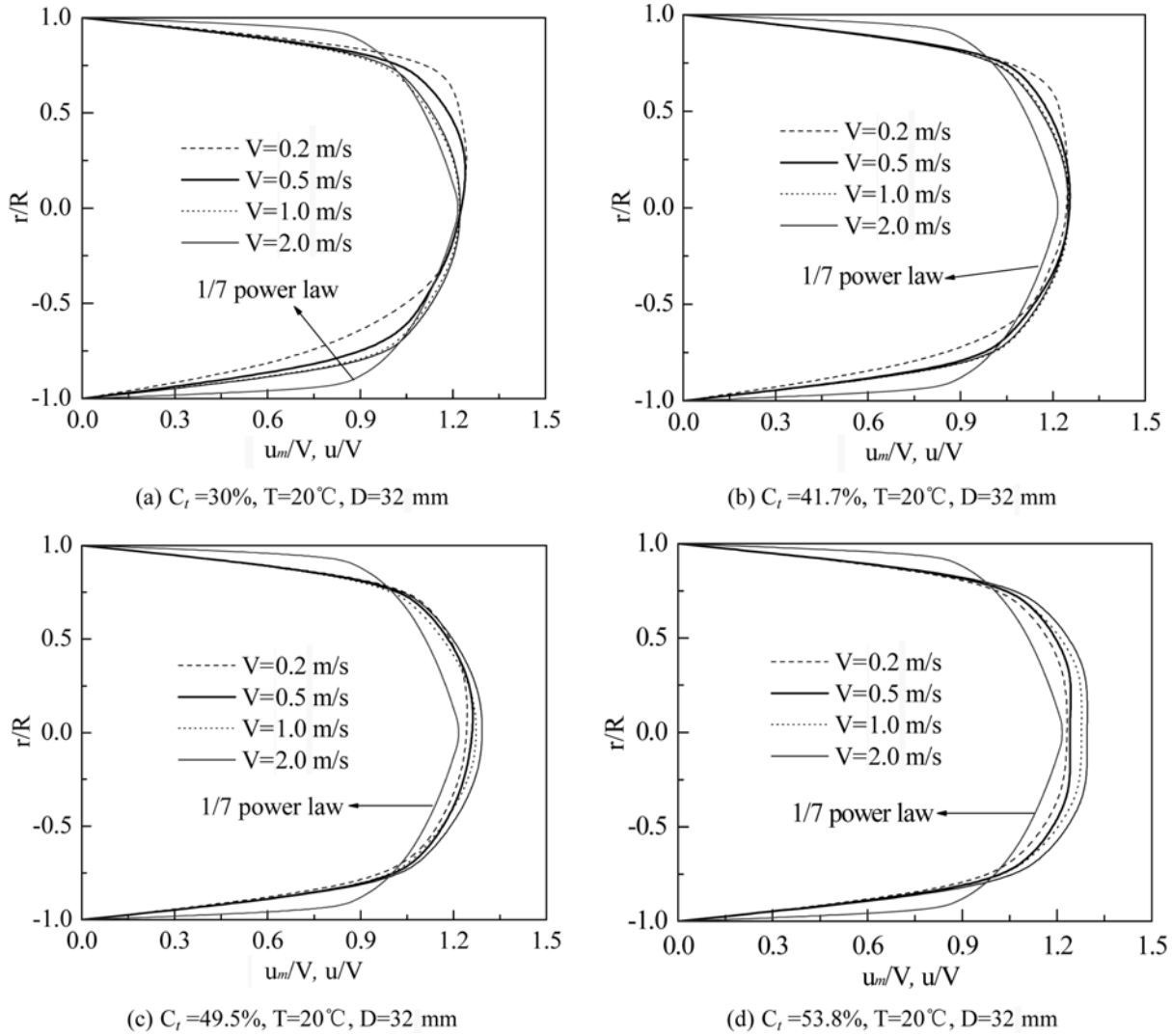

Fig. 9. Axial velocity distribution along the vertical diameter.

ticles along vertical diameters vary considerably due to gravitational force at low influx velocity and they show a similar distribution with those of total volume concentration. However, 65 μm particles are distributed more uniformly at all heights expect for in the low part of pipelines. This distribution pattern is similar to those of dense slurries with double species having different particle size or density showed by experiments [16] as well as by CFD simulation [25]. The volume ratio of coarse to fine particles in low parts of pipelines shows significant deviation from influx value at low influx velocity. The more coarse particles accumulate in the low part of the pipeline, the more fine particles are piled out of the same region. This suggests that the solid distribution is not only affected by gravitational effects but also by strong particle-particle interactions between fine and coarse particles. With increase of influx velocity and total influx concentration, inhomogeneity of the constituent particle concentration profile is gradually reduced. When total influx concentration is beyond 50%, the flow almost becomes homogeneous regime with constituent particles being distributed uniformly at all influx velocities investigated.

As expected, the calculated results suggest that the total volume concentrations and constituent particle concentrations in the horizontal diameter remain uniform irrespective of influx velocity and total influx concentration. This conclusion is consistent with the experimental results from literature [16].

4. Velocity Profile

The addition of solid particles to turbulent liquid flow will modify velocity distribution of the flow. Fig. 9(a)-(d) depict the calculated dimensionless axial velocity profiles along the vertical diameters in fully developed region for slurries at different influx velocities. Here the dimensionless velocities are calculated in terms of ratio of mean velocity of the mixture to influx velocity, u_m/V. From Fig. 9(a)-(b), one can observe that the axial velocity profiles are obviously asymmetric along the vertical diameter in flow of 30% slurries and 41.7% slurries when influx velocity is lower than 0.5 m/s. The velocity profiles in lower part of the pipe centerline would be lower than those in the upper part. This is expected because the solid concentrations in the lower part of the pipelines are much higher than those in the upper part based on the effects of gravity, and more dissipated energy will be consumed to drive particles for water in the lower part, which results in a lower velocity in this area. With increase of

influx velocity, the degree of asymmetry of the velocity profile decreases. For slurries with single solid phase, the degree of asymmetry of axis velocity along the vertical diameter is a measurement of the uniformity of solid particle concentration distribution in the vertical plane [5]. However, for slurries with solid phase having bimodal distribution, the asymmetry of the axis velocity along the vertical diameter is also affected by the local volume ratio of coarse to fine particles. From Fig. 8(a)-(b) and Fig. 9(a)-(b), it is clear that there are fairly high gradients of total volume concentration in the lower and upper parts of pipelines for 30% and 41.7% slurries at influx velocities of 1.0 m/s and 0.5 m/s, respectively. However, the velocity profiles along vertical diameters become almost symmetric. This is mainly due to the fact that the difference in volume ratio of coarse to fine particles between the lower and upper parts of pipelines reduces the asymmetry of the velocity profile along the vertical diameter which arises from nonuniformity of the total volume concentration distribution in slurries. For 49.5% slurries and 53.8% slurries, the velocity profiles along vertical diameters are symmetric even at the lowest influx velocity studied.

For comparison, the velocity profile of single phase turbulent flow is also given by one-seventh power law $u/V=60/49(1-(r/R))^{1/7}$ in Fig. 9(a)-(d). Single phase turbulent flow is characterized for its high velocity gradient very near the pipe wall and an approximately uniform flow velocity across the rest of the pipe. The velocity profiles of 30% slurries in fully developed suspended flow show less velocity gradient near the pipe wall and more velocity gradient in the region near the centerline than single phase turbulent flow. As the solid concentration is increased, the velocity and its gradients increase more near the centerline as a result of further reduced turbulence intensity. As mentioned above, the flow of 53.8% slurries becomes under control of the solid motion, and the velocity gradient disappears in the region near the centerline.

Fig. 10 shows the comparison of axial velocity distribution along vertical diameter with that along horizontal diameter for 49.5% coal-water slurry at influx velocity of 0.5 m/s. Clearly, the axial velocity profile along the horizontal diameter is symmetric as a result of invariance of total volume concentration and constituent particle concentration. The axial velocity distribution along the vertical diameter is much different from that along the horizontal one, though the asymmetry of velocity profile along the vertical diameter is reduced by the difference in local volume ratio of coarse to fine particles between the lower and upper parts of pipelines. The velocity and its gradient along the horizontal diameter are much higher than those along the vertical diameter in a short region near the pipe wall, while in the region near the centerline, the velocity along the horizontal diameter is higher and distributed more uniformly. This makes the constant velocity contour curve in vertical plane become oblate, as shown by Fig. 7(d). For slurries with single solid phase, the velocity profiles along the vertical and horizontal diameters are symmetric and exactly the same in a homogeneous flow regime. Discrepancies between the two profiles would appear for nonuniform distribution of volume concentration in slurry flow. However, for our slurries with solid phase having bimodal distribution, the discrepancies between the two profiles are the synthesis results of nonuniform distribution of total volume concentration and the differences in local volume ratio of coarse to fine particles between the lower and upper parts of pipelines.

5. Effects of Grain Composition

It is very difficult to investigate the effects of grain composition on flow behaviors of CWSs by experiments on our pilot scale transport apparatus, but it is easy to obtain them in numerical investigation. Numerical investigations of effects of grain composition were carried out by comparing numerical results of our double-solid-phase method with those of single-solid-phase method in the same framework of Eulerian multiphase approach. In the single-solid-phase method, the coal particles with bimodal distribution are considered as single solid phase, which has the same mean particle diameter as solid phases in our double-solid-phase methods. Fig. 11 shows the comparison of experimental pressure gradients with numerical results obtained by single/double-solid-phase methods for 41.7% slurries. The numerical pressure gradients by double-solid-phase methods are in good agreement with the experimental data. How-

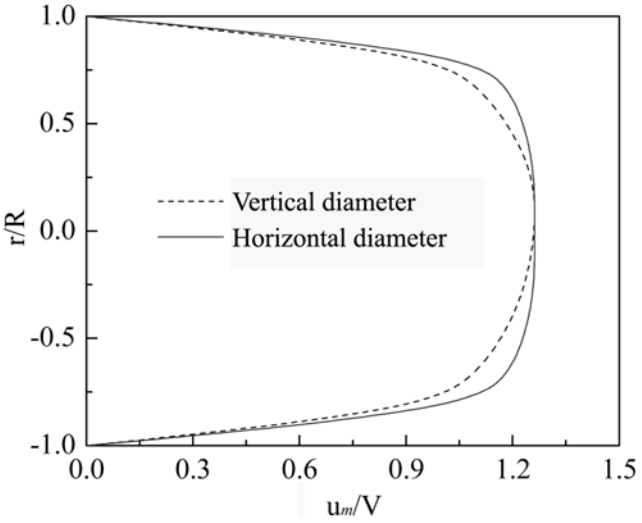

Fig. 10. Comparison of axial velocity distribution along vertical diameter with that along horizontal diameter (C_t=49.5%, V=0.5 m/s, T=20 °C, D=32 mm).

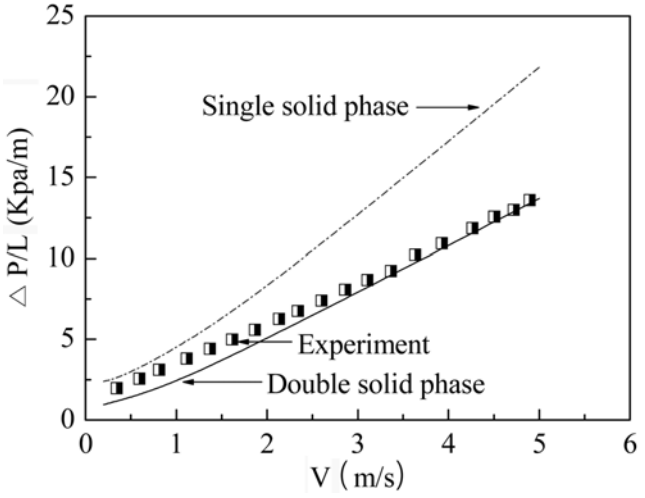

Fig. 11. Comparison of experimental pressure gradients with numerical results obtained by single/double-solid-phase methods (C_t=41.7%, T=20 °C, D=32 mm).

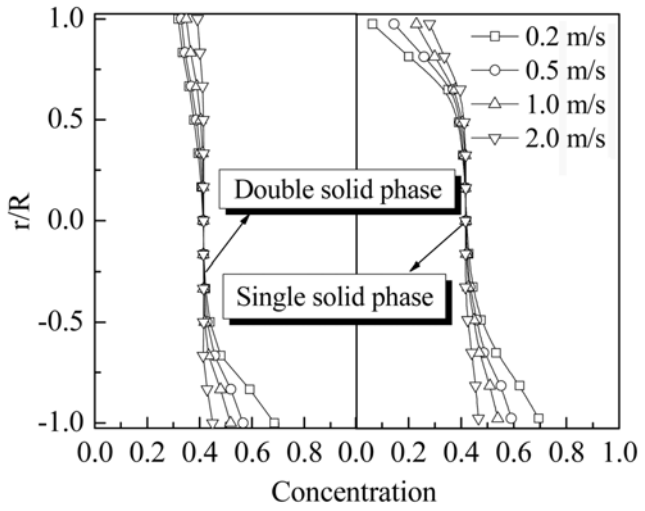

Fig. 12. Numerical concentration profiles along vertical diameter obtained by single/double-solid-phase methods (C_t=41.7%, T=20 °C, D=32 mm).

ever, the single-solid-phase method *overestimates* the values of pressure drops, especially at high velocity. This suggests that fluidity of slurries filled with both fine and coarse particles is enhanced by fine particles filling up the interspaces formed by coarse particles. Fig. 12 presents numerical (total) volume concentration profiles along the vertical diameters obtained by single/double-solid-phase methods for 41.7% slurries. Obviously, the solid phases of slurries filled with fine and coarse coal particles are distributed more uniformly than those of slurries filled with single solid phase at all influx velocities, especially on the top of pipelines. It is concluded that the arrangement of particles in the mixture is improved with the fine particles filling the void spaces between the coarse particles, and the stability of slurries is enhanced by the strong particle-particle interactions between fine and coarse particles. This also well explains why lower energies are consumed in flow of slurries with solid phase having bimodal distribution.

CONCLUSION

The Eulerian multiphase approach with kinetic theory of granular flow was applied to predict flow behaviors of coal-water slurries in horizontal pipelines. The numerical investigations have displayed some important slurry flow characteristics, such as constituent particles concentration and velocity distribution as well as pressure gradients. Based on our experimental and numerical investigations, the following conclusions can be made:

(1) The model proposed here captures the main features of solid-liquid flow of super dense coal-water slurries in horizontal pipelines over a wide range of operating conditions. Numerical predictions for the pressure gradients are in good agreement with the experimental data when total influx concentrations are not more than 50%.

(2) The total and constituent particle volume concentration profiles along the vertical diameter are affected not only by gravitational force but also by strong particle-particle interactions between fine and coarse particles. The concentration of coarse particles along vertical diameter varies considerably at lower influx velocity and concentration, while the fine particles are distributed more uniformly in the vertical plane. The solid phases are distributed more uniformly at higher influx velocity and solid concentration.

(3) The axial velocity profiles along vertical diameter are affected not only by the total volume concentration distribution but also by the local volume ratio of fine to coarse particles. The axial velocity distribution along the vertical diameter usually shows great discrepancies from that along the horizontal diameter.

(4) Coal-water slurries filled with binary solid phase are distributed more uniformly and exhibit higher fluidity than slurries with single solid phase.

ACKNOWLEDGMENT

This study was funded by the State Basic Research Development Program (973 Plan) of China (No. 2004CB217701).

NOMENCLATURE

C_D : drag coefficient
C_t : total volume concentration [%]
D : test pipe diameter [mm]
D_{fsi} : granular energy dissipation rate [kg/s^{3}m]
d : particle diameter [m]
e : restitution coefficient
g : acceleration gravity [m/s^2]
g_0 : radial distribution function
I : unit tensor
$K_{\Theta si}$: granular conductivity
k : turbulence kinetic energy [m^2/s^2]
L : length of pipe [mm]
P : pressure [kg/m·s^2]
R : test pipe radius [mm]
r : radius [m]
T : slurry temperature [°C]
u : velocity vector
u : velocity [m/s]
V : influx velocity [m/s]

Greek Letters

α : volume fraction
β : inter-phase drag coefficient [kg/m^3·s]
λ : bulk viscosity [kg/m·s^{-1}]
μ : viscosity [kg/m·s^{-1}]
$\mu_{t,f}$: turbulence viscosity of liquid [kg/m·s^2]
ρ : density [g/cm^3]
ε : dissipation rate of k [m^2/s^3]
φ : specularity coefficient
τ : viscous stress tensor [kg/m·s^{-2}]
$\gamma_{\Theta si}$: collision dissipation of energy [kg/s^{3}m]
Θ_s : granular temperature [m^2/s^2]
ϕ_{fsi} : transfer rate of kinetic energy [kg/s^{3}m]

Subscripts

f : fluid
ij : between ith and jth solid phase

m : mean value of the mixture
max : maximum
si, sj : i^{th} or j^{th} component of solid phase

REFERENCES

1. Y. C. Choi, T. J. Park, J. H. Kim, J. G. Lee, J. C. Hong and Y. G. Kim, *Korean J. Chem. Eng.*, **18**, 493 (2001).
2. S. K. Lahiri and K. C. Ghanta, *The 17th international conference on the hydraulic transport of solids*, Cape town, Southern African, 149 (2007).
3. N. Z. Beata and Z.Wojciech, *International Journal of Refrigeration*, **29**, 429 (2006).
4. F. L. Hsu, Ph.D. thesis, AAI8726087, University of Illinois at Chicago, Chicago, IL (1987).
5. M. H. Assar, Ph.D. thesis, AAI9720393, Case Western Reserve University, OH (1996).
6. J. Ling, P. V. Skudarnov, C. X. Lin and M. A. Ebadian, *International Journal of Heat and Fluid Flow*, **24**, 389 (2003).
7. C. X. Lin and M. A. Ebadian, *Computers & Fluids*, **37**, 965 (2008).
8. J. Xu, A. Rouelle, K. M. Smith, D. Celik, M. Y. Hussaini and S. W. Van Sciver, *Cryogenics*, **44**, 459 (2004).
9. T. C. Jack, T. Fariborz, E. Renaud, E. Naoko and R. G. John, *Chemical Engineering Science*, **62**, 6334 (2007).
10. L. Paola, D. F. Renzo, P. Roberta and O. Olumuyiwa, *Powder Technology*, **167**, 94 (2006).
11. R. Panneerselvam, S. Savithri and G. D. Surender, *Chemical Engineering Journal*, **132**, 159 (2007).
12. S. Roy and M. P. Dudukovic, *Industrial and Engineering Chemistry Research*, **40**, 5440 (2001).
13. Y. Cheng and J. Zhu, *Canadian Journal of Chemical Engineering*, **83**, 177 (2005).
14. Y. B. Liu, J. Z. Chen and Y. R.Yang, *Journal of Zhejiang University (Engineering Science)*, **40** (2006).
15. O. Shinichi, S. David and O. Kohei, *Chemical Engineering Science*, **61**, 3714 (2006).
16. D. R. Kaushal, S. Kimihiko, T. Takeshi, F. Katsuya and T. Yuji, *International Journal of Multiphase Flow*, **31**, 809 (2005).
17. P. V. Skudarnov, C. X. Lin and M. A. Ebadian, *Journal of Fluids Engineering*, **126**, 125 (2004).
18. D. Gidaspow, *Multiphase flow and fluidization: Continuum and kinetic theory descriptions*, Academic Press, New York (1994).
19. Y. R. He, H. S. Chen, Y. L. Ding and B. Lickiss, *Chemical Engineering Research and Design*, **85**, 963 (2007).
20. J. T. Jenkins and S. B. Savage, *J. Fluid Mech.*, **130**, 187 (1983).
21. J. Ding and D. Gidaspow, *AIChE J.*, **36**, 523 (1990).
22. C. K. K. Lun, S. B. Savage, D. J. Jeffrey and N. Chepurniy, *Journal of Fluid Mechanics*, **140**, 223 (1984).
23. S. Ogawa, A. Umemura and N. Oshima, *Z. Angew. Math. Phys.*, **31**, 483 (1980).
24. P. C. Johnson and R. Jackson, *J. Fluid Mech.*, **176**, 67 (1987).
25. J. Yang and R. J. Chalaturnyk, *3rd international conference on computational methods in multiphase flow*, Xi'an (2005).